CEAS Aeronautical Journal
https://doi.org/10.1007/s13272-026-01035-0

ORIGINAL PAPER

Possibilities and limits of contrail avoidance through aircraft engine design for kerosene- and hydrogen-fuelled engines

Julian Callard[1] · **Daniel Weintraub**[1] · **Peter Jeschke**[1]

Received: 28 April 2026 / Revised: 30 September 2026 / Accepted: 27 October 2026
© The Author(s) 2026, modified publication 2026

Abstract

In this paper, we present a thermodynamic cycle-based analysis of the effect of aircraft engine design and fuel selection on contrail formation, which is evaluated using the Schmidt–Appleman criterion (SAC). Our goal is to examine the possibilities and limits of contrail avoidance to reduce the climate impact of aviation. We use the gas turbine performance software GasTurb to study geared-turbofan and open-rotor engine designs for contemporary short- to medium-range aircraft. The design parameters are overall pressure ratio, burner exit temperature, and, for the geared-turbofan, the design bypass ratio. We vary these parameters in wide ranges to cover all technically feasible engine designs. We find that contrail formation at current cruise altitudes cannot be avoided with the examined contemporary and future engine cycles. In the best case, the contrail formation altitude is increased by just over 230 m. This comes with a significant engine efficiency penalty. In contrast, future, more efficient engine cycles will decrease the contrail formation altitude, leading to the formation of more contrails. When using hydrogen as fuel instead of kerosene, contrails form at approximately 1.6 km lower altitudes according to the Schmidt–Appleman criterion. We thus find that it is practically impossible to avoid contrail formation, as predicted by the SAC, using the engine cycles and fuels examined in this paper. Operational contrail avoidance measures like cruise altitude adjustment or flying around ice-supersaturated atmospheric layers present themselves as more practicable.

Keywords Contrails · Performance calculation · Engine cycle adaptation

List of symbols

ALT	Altitude (m)
EI_{H2O}	Water emission index (–)
FHV	Fuel heating value ($MJ\,kg^{-1}$)
C_P	Specific heat capacity at constant pressure ($Jkg^{-1}\,K^{-1}$)
F_N	Net thrust (kN)
G	Mixing line slope ($Pa\,K^{-1}$)
P_D	Partial pressure of water vapour (Pa)
T	Total temperature (K)
T_s	Static temperature (K)
V_0	Aircraft velocity (ms^{-1})
W	Mass flow ($kg\,s^{-1}$)
M	Mach number (–)

Greek letters

η_o	Overall engine efficiency (–)
ε	Ratio of molar masses of water and dry air (–)

Subscripts

1, 2, ..	Thermodynamic stations, Figs. 3 and 4
amb	Ambient
C	Critical
cruise	Cruise
F	Fuel

Abbreviations

FPR	Fan pressure ratio (–)
BPR	Bypass ratio (–)

✉ Julian Callard
callard@ist.rwth-aachen.de

Daniel Weintraub
weintraub@ist.rwth-aachen.de

Peter Jeschke
jeschke@ist.rwth-aachen.de

[1] Institute of Jet Propulsion and Turbomachinery, RWTH Aachen University, Templergraben 55, 52062 Aachen, Germany

Published online: 05 November 2026

CO_2	Carbon dioxide
GTF	Geared-turbofan
HPC	High-pressure compressor
HPT	High-pressure turbine
ICAO	International Civil Aviation Organization
IPC	Intermediate-pressure compressor
IPT	Intermediate-pressure turbine
ISA	International standard atmosphere
LPT	Low-pressure turbine
nvPM	Non-volatile particulate matter
OPR	Overall pressure ratio
OR	Open-rotor
RF	Radiative forcing
RPM	Revolutions per minute (1 min^{-1})
SAC	Schmidt–Appleman criterion
SFC	Thrust-specific fuel consumption ($g\,kN^1\,s^{-1}$)
VIGV	Variable inlet guide vane
vPM	Volatile particulate matter
WET	Water-enhanced turbofan

1 Introduction

Aircraft-induced contrails contribute significantly to the radiative forcing (RF) of aviation and thereby affect the climate. As part of the broader non-CO_2 effects, they are estimated to contribute at least as much—and possibly up to twice as much—to aviation's RF as CO_2 emissions [1–3]. They frequently form behind aircraft in the upper troposphere and lower stratosphere [3]. Schmidt [4] and Appleman [5] developed the first thermodynamic theories on contrail formation. Schumann further developed these theories into the Schmidt–Appleman criterion (SAC). The contrail prediction accuracy of the SAC has been shown in test flight campaigns [6, 7].

Contrails form when humid engine exhaust gases mix with sufficiently cold ambient air. The mixing represents the necessary condition for contrail formation. If saturation with respect to liquid water is reached in the exhaust plume, water vapour from the combustion of fuel in the engine condenses on the condensation nuclei present in the exhaust stream. The condensed water vapour forms liquid water droplets, which immediately freeze to form contrails [3]. Reaching saturation constitutes the sufficient condition for contrail formation and is described by the Schmidt–Appleman criterion (SAC) formulated by Schumann [6].

In a dry atmosphere, the contrails usually dissipate quickly after forming. In atmospheric layers that are supersaturated with respect to ice, contrails do not dissipate and can remain in the atmosphere for longer. Such persistent contrails can begin to grow into contrail-induced cirrus clouds [6, 8] that reflect long-wavelength radiation back down to Earth, thereby contributing the non-CO_2 RF [9]. The RF mechanisms of contrails and methods to reduce their climate impact are the subject of ongoing research [3, 8–13].

Recent work on the impact of volatile particulate matter in the exhaust stream suggests that in a low-soot regime, ice nucleation occurs on volatile sulfate aerosols, volatile lubrication oil particles, and organic volatile particles. In a high-soot regime, the produced soot and other non-volatile particulate matter (nvPM) act as ice nuclei. Droplets formed on volatile particles then freeze homogeneously. The crystals then grow from the uptake of ambient water vapour, the same way as the heterogeneously nucleated soot ice particles [14–16]. The ice particle numbers in the lean-burn, low-soot modes in these studies are similar to those in a forced rich-burn, high-soot mode [16].

Contrail mitigation comprises technical and operational strategies. Operational strategies typically involve avoiding the ice-supersaturated areas by flight re-routing or level changes [17, 18]. The main difficulty faced by these approaches is the detection of and re-routing around ice-supersaturated atmospheric layers. This is avoided if contrails are prevented on a technical level in the engine itself.

In previous work, we investigated the potential for contrail mitigation by retrofitting existing engines. We varied the bypass and core nozzle areas, high- and low-pressure turbine capacities, a handling bleed, and a high-pressure bleed [19]. The method we used relies on reducing the engine efficiency temporarily, which increases the exhaust gas temperature, thereby increasing the altitude where contrails just begin to form (critical altitude) [17, 19]. We found that the critical altitude can be increased by around 200 m for a contemporary geared-turbofan engine at a cruise altitude of 10 km. This relatively small increase in critical altitude comes at the prohibitive cost of an increase in thrust specific fuel consumption (SFC) of 35%, with significantly increased turbine temperatures [19]. The examined engine design and operating point changes did not prevent contrails from forming. Similarly, Haglind [20] found that utilising variable inlet guide vanes in a turbofan engine increased the critical altitude of contrail formation by 300 m. This was accompanied by a 45% increase in SFC. Together, these results show that retrofitting existing engines in these ways is not a viable solution for reducing contrail formation during cruise.

The critical altitude for contrail formation further depends on the fuel type [6]. Alternative fuels with higher hydrogen content, such as methane and hydrogen, which are gaining relevance for climate-neutral air travel, produce less CO_2 but more water vapour during combustion. This can lead to contrail formation at lower altitudes compared to fuels

with lower hydrogen content [17]. This may be mitigated by removing water vapour from the exhaust gas [21–23].

In this paper, we extend our previous work by exploring a wide engine design space to make a general statement on the impossibility of technical contrail avoidance by means of engine design. The study covers a range of aircraft propulsion cycles, from early turbofan engines to advanced concepts anticipated for 2050 and beyond, including open-rotor engines and high-bypass-ratio turbofans. We focus on three key design parameters: bypass ratio, burner exit temperature, and overall pressure ratio. Furthermore, we investigate how the use of hydrogen and kerosene influences the contrail formation altitude of each engine cycle at the design point.

2 Theory

In this section, we outline the thermodynamic theory to describe contrail formation. This brief summary is largely based on the work of Schumann [6], building on our previous paper [19].

According to the SAC, contrails form if the exhaust plume, while being progressively diluted by mixing with ambient air, becomes saturated or supersaturated with respect to liquid water. As shown in Fig. 1, this mixing process starts out as a straight line in a partial pressure of water vapour versus temperature diagram. The underlying assumptions are: ideal mixing, constant specific heat capacity, isobaric conditions, and that the partial pressure of water vapour is much smaller than the ambient pressure. This *mixing line* connects the engine exhaust conditions above and

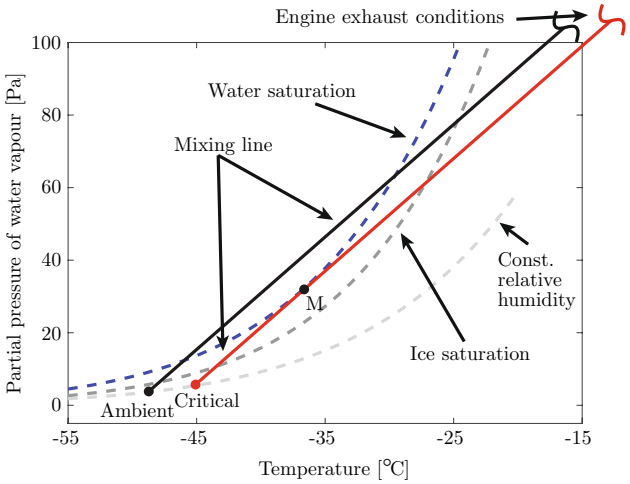

Fig. 1 Partial pressure of water vapour versus temperature graph, derived from Schumann [7]. The red mixing line is chosen so it touches the water saturation line, shown in blue. Here, contrails just begin to form at point M for a critical ambient temperature at point C. Persistent contrails form if the ambient conditions are above the ice saturation line, shown in dark grey

to the right of the diagram to the ambient conditions in the bottom left. Contrails can begin to form when the mixing line crosses the water saturation curve. If a mixing line, as shown in red in Fig. 1, just touches the water saturation curve, contrails will just begin to form. Hence, contrails will form for a constant ambient humidity with respect to water, if the ambient temperature is below a critical temperature.

According to Schumann, the gradient of the exhaust gas-ambient air mixing line can be expressed as

$$G = \frac{\Delta P_D}{\Delta T} = \frac{P_{\text{amb}} \text{EI}_{\text{H2O}} C_P}{\varepsilon \, \text{FHV}(1-\eta_o)} \tag{1}$$

where P_{amb} is the ambient pressure, EI_{H2O} is the water emission index in $\text{kg}_{\text{water}}/\text{kg}_{\text{fuel}}$, C_P is the specific heat capacity of air at constant pressure. ε denotes the ratio of the molar masses of water vapour and dry air, given as $\varepsilon = 0.622$. FHV is the fuel heating value and η_o the overall efficiency of the engine. In Eq. 1, the ratio of the water emission index and the fuel heating value is also referred to as the energy-specific water emission index

$$\text{Energy-specific emission index} = \frac{\text{EI}_{\text{H2O}}}{\text{FHV}} \tag{2}$$

It is a fuel-specific value and has a significant influence on the mixing line gradient. Kerosene has an energy-specific emission index of around 0.029 kg(H2O)/MJ, while that of hydrogen is around 0.078 kg(H2O)/MJ. This larger energy-specific emission index causes an increased mixing line gradient for hydrogen in the SAC, leading to a predicted increase in contrail formation for hydrogen.

The overall efficiency can be expressed as

$$\eta_o = \frac{F_N V_0}{W_F \text{FHV}}, \tag{3}$$

with the net thrust F_N, aircraft velocity V_0, and fuel flow W_F. Schumann [7] describes the influence of the engine efficiency on contrail formation as the η-effect and derives the relationship from an energy budget in a frame of reference fixed to the ambient air. The SAC is thus a strictly thermodynamic theory of contrail formation.

As described in the introduction, the SAC is validated with respect to kerosene in flight test campaigns. The contrail formation is predicted correctly without taking the micro-physical processes involved into account. The SAC has not yet been validated with respect to hydrogen. We make the assumption that the SAC can also be used for the contrail prediction of hydrogen-burning engines. Therefore, the studies performed in this paper offer an indication on the contrail formation of the aircraft engine cycles examined.

Although our study addresses only the formation of contrails and not their impact on the climate, it is worth noting at this point that the radiative forcing of contrails, and thus their climate impact, depend strongly on their optical properties, particularly their optical depth, as well as on their microphysical characteristics. Contrail formation is governed by complex physical processes and is influenced not only by fuel composition, but also by the properties and number of exhaust particles as well as the dynamics of ice nucleation [12, 13, 24–26]. Therefore, an engine configuration associated with more frequent contrail formation may still lead to a similar or even reduced climate impact compared with a configuration that produces fewer contrails, if the resulting contrails are optically thinner, shorter-lived, or otherwise differ in their microphysical properties.

2.1 Critical altitude

The critical temperature $T_{s,C}$ is the highest ambient temperature at which the exhaust plume reaches liquid-water saturation during mixing with ambient air. As discussed above, for ambient temperatures $T_{\mathrm{s,amb}} < T_{s,C}$, the Schmidt–Appleman criterion for contrail formation is fulfilled, i.e., we expect contrails to form. To facilitate the comparison of different engine concepts, we translate the temperature margin $T_{\mathrm{s,amb}} - T_{s,C}$ into an equivalent change in critical altitude, assuming the ICAO standard atmosphere below 11 km [27], as shown in Fig. 2. Using the standard tropospheric lapse rate of 6.5 K/km, this yields

$$\Delta \mathrm{ALT}_C = (T_{\mathrm{s,amb}} - T_{s,C}) \frac{1000\,\mathrm{m}}{6.5\,\mathrm{K}} . \tag{4}$$

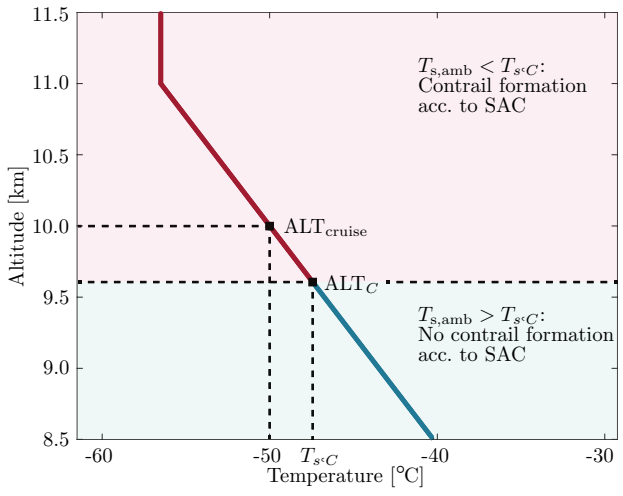

Fig. 2 Altitude versus temperature graph. The temperature line is calculated using the ICAO standard atmosphere equations [27]. The critical altitude is calculated for $\eta_o = 0.37$ and the energy-specific emission index of kerosene of 0.029 kg(H2O)/MJ at a cruise altitude of 10 km and the ambient humidity with respect to water of 60%

Here, $\Delta \mathrm{ALT}_C$ represents the altitude change, relative to the considered cruise condition, required for the standard-atmosphere ambient temperature to reach the SAC threshold. The corresponding critical altitude is

$$\mathrm{ALT}_C = \mathrm{ALT}_{\mathrm{cruise}} + \Delta \mathrm{ALT}_C . \tag{5}$$

Thus, ALT_C is not a direct output of the Schmidt–Appleman criterion, but an ISA-based representation of the SAC temperature threshold. We use this quantity as a metric for comparing the influence of the investigated thermodynamic cycles and fuels on contrail formation conditions. It is important to point out that the real atmospheric conditions are subject to regional and seasonal changes. This temperature fluctuation strongly influences the critical altitude. The absolute values of the critical altitude and the difference in critical altitude calculated in this study are a qualitative indication of the contrail formation of an engine configuration. For any given flight the actual critical altitude could be higher or lower, depending on the given lapse rate and ambient temperature.

3 Methodology

We consider the short- to medium-range aircraft class use-case (Airbus A320neo) as short- and medium-range air traffic comprises 96% of the total air traffic volume [28]. The studies are performed for cruise flight, as contrails typically form during this flight phase.

We first define a modern geared-turbofan engine, which serves as the reference engine for the study. Starting from this reference configuration, we generate generic geared-turbofan cycles by varying the bypass ratio, overall pressure ratio, and burner exit temperature. We then derive the open-rotor engine from the same reference geared turbofan by adding a power-turbine spool. For the open-rotor configuration, we vary the overall pressure ratio and burner exit temperature. Unless explicitly stated otherwise, all remaining parameters are kept constant.

3.1 Geared-turbofan modelling

The common cruise design point used for the reference engine and all subsequent design-space studies is given in Table 1.

The reference engine is a generic modern two-spool geared-turbofan engine in the 120 kN thrust class, representative of current-generation narrow-body propulsion systems. Its main design characteristics are selected based on publicly available data for engines of this class, such as the Pratt & Whitney PW1100G family [29, 30]. At the cruise

Table 1 Cruise design point used for the reference engine configuration and all design-space studies

Design point parameter	Value
Altitude	10 km
Mach number	0.78
Net thrust per engine	25 kN
ISA conditions	$\Delta T = 0$

Table 2 Reference GTF engine design parameters at the cruise design point given in Table 1

Engine design parameters	Value
Design bypass ratio	10.7
Engine mass flow W_2	198.67 kg s^{-1}
Outer fan pressure ratio	1.57
Inner fan pressure ratio	1.46
Booster pressure ratio	2.56
High-pressure compressor pressure ratio	13.6
Burner exit temperature	1700 K
Polytropic compressor and turbine efficiency	0.9
Power offtake	0 kW
LP and HP spool mechanical efficiency	0.995
HP turbine stages	2
HP stage 1 NGV cooling flow	5% W_{25}
HP stage 1 rotor cooling flow	5% W_{25}
HP stage 2 NGV cooling flow	3% W_{25}
HP stage 2 rotor cooling flow	3% W_{25}
LP turbine stages	3
LP stage 1 guide vane cooling flow	1% W_{25}
LP stage 1 rotor cooling flow	0.5% W_{25}

The polytropic efficiency is applied to all compressors and turbines

design point, the required net thrust is 25 kN per engine. The corresponding reference engine design parameters are listed in Table 2. At this operating point, the engine has a specific fuel consumption of 14.47 g/(kNs).

Starting from this reference configuration, we generate the generic GTF cycles investigated in the design-space exploration by systematically varying selected design parameters. The thermodynamic stations and bleed locations of the GTF configuration implemented in GasTurb are shown in Fig. 3.

For each GTF cycle, the prescribed design parameters are the bypass ratio, overall pressure ratio (OPR), and burner exit temperature T_4. The booster pressure ratio is kept constant, while the high-pressure compressor pressure ratio is adjusted to meet the target OPR. The outer fan pressure ratio is set to achieve the optimal bypass-to-core nozzle exit velocity ratio of

$$(V_{18}/V_8)_{\mathrm{id}} = 0.82\,. \tag{6}$$

The inner fan pressure ratio is then calculated as

$$\mathrm{FPR}_{\mathrm{inner}} = 1 + 0.8(\mathrm{FPR}_{\mathrm{outer}} - 1)\,. \tag{7}$$

The engine mass flow is subsequently adjusted so that each cycle satisfies the required net thrust of 25 kN. All engine cycles are calculated twice, once with kerosene and once with hydrogen.

The GTF design parameters varied in this study and their respective bounds are given in Table 3.

The analysis is limited to design-point calculations, with the required net thrust kept constant at $F_N = 25\,\mathrm{kN}$ for all configurations. Off-design performance and aircraft-level effects associated with changes in engine size and mass are

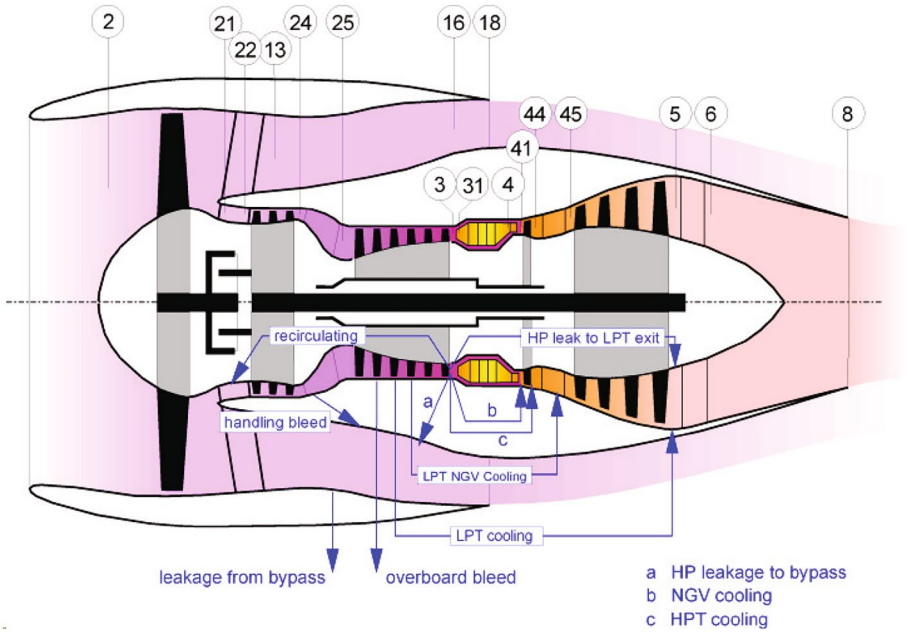

Fig. 3 Thermodynamic stations and bleed locations of the GTF engine configuration in GasTurb

Table 3 Varied GTF engine design parameters and bounds at the cruise design point

Engine design parameter	Lower limit	Upper limit
Design bypass ratio	1	15
Overall pressure ratio	30	70
Burner exit temperature	1450 K	1950 K

The parameter limits are chosen to represent current and potential future engine cycles

not considered. In line with the focus on first-order trends, we also neglect secondary effects such as changes in component efficiency due to engine resizing and changes in cooling-flow requirements with burner exit temperature. These effects are not expected to alter the main trends discussed in the following. At the assumed cruise condition of 10 km altitude, all investigated configurations satisfy the Schmidt–Appleman criterion. The analysis therefore focuses on how the investigated design parameters shift the critical altitude across the design space.

3.2 Open-rotor modelling

The open-rotor engine cycles are also derived from the reference geared-turbofan, with an added power-turbine spool. This configuration retains the booster and high-pressure-compressor arrangement of the reference GTF while introducing the free-speed design flexibility characteristic of power-turbine-driven open-rotor concepts. The corresponding GasTurb configuration is shown in Fig. 4.

The open-rotor design space follows the same approach as the GTF design space, except for the bypass ratio. The examined open-rotor design parameters are the OPR and burner exit temperature T_4. Their respective bounds are given in Table 4.

Table 4 Varied open-rotor engine design parameters and bounds at the cruise design point

Engine design parameter	Lower limit	Upper limit
Overall pressure ratio	30	70
Burner exit temperature	1450 K	1950 K

The parameter limits are chosen to represent current and potential future engine cycles

The remaining relevant open-rotor design parameters, which are kept constant throughout the design space exploration, are listed in Table 5.

Both the GTF and open-rotor models are available from the corresponding author upon request.

3.3 Toolchain setup

The thermodynamic engine cycles are generated in GasTurb using the batch-job functionality [31–33]. This approach is used to vary the design parameters of the generic two-spool GTF and three-spool OR configurations. The required thermodynamic quantities for the calculation of the SAC are exported from GasTurb and processed in MATLAB.

The Schmidt–Appleman criterion is implemented in MATLAB, which is also used for post-processing the design-space data. The water and ice saturation vapour pressure curves are calculated using the formulations presented by Sonntag [34].

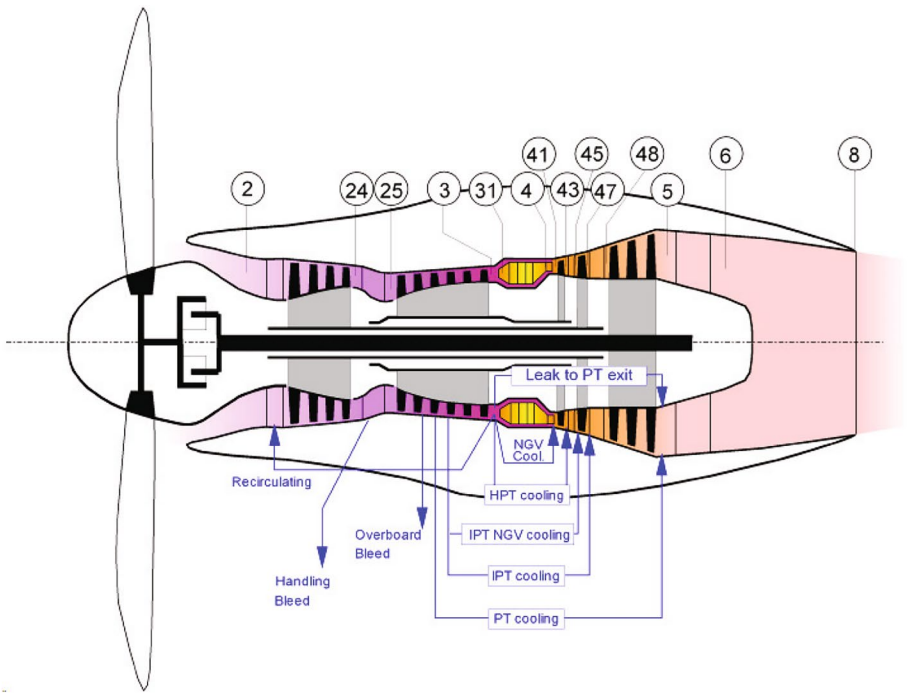

Fig. 4 Thermodynamic stations and bleed locations of the open-rotor engine configuration in GasTurb

Table 5 Constant open-rotor engine design parameters at the cruise design point

Engine design parameter	Value
Booster pressure ratio	2.5
Polytropic efficiency	0.9
Power offtake	0 kW
HP, IP, and PT spool mechanical efficiency	0.995
HP turbine stages	1
HP guide-vane cooling flow	5% W_{25}
HP rotor cooling flow	3% W_{25}
IP turbine stages	1
IP guide-vane cooling flow	1% W_{25}
IP rotor cooling flow	1% W_{25}
PT turbine stages	3
PT rotor cooling flow	0.5% W_{25}
Rotor diameter	3 m
Rotor RPM	1230 min^{-1}
Advance ratio	3.8

The polytropic efficiency is applied to all compressors and turbines

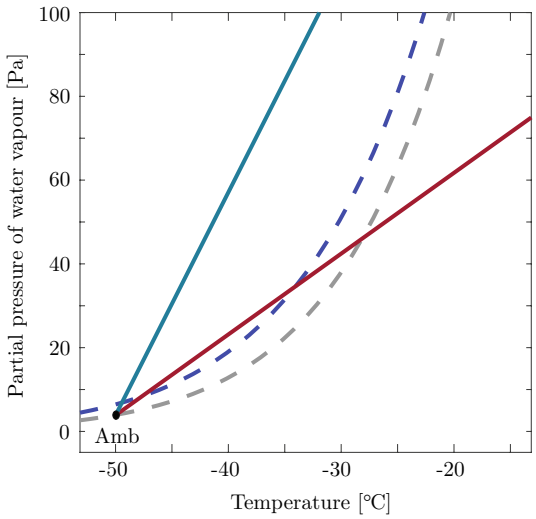

Fig. 5 Mixing lines for the reference configuration for kerosene (red) and hydrogen (blue) at the reference cruise conditions of ALT = 10 km, M = 0.78, F_N = 25 kN. The reference engine produces contrails for both fuels at this altitude

4 Results

The study results are presented in this section, starting with the reference GTF configuration. Persistent contrails only form if the atmosphere is saturated with respect to ice. This is the case for relative humidity with respect to water of around 60% for the studied temperature range. We therefore evaluated all cases at 60% relative humidity with respect to water to determine whether whether persistent contrails can form for the examined engine cycles. The critical altitude for each configuration was calculated according to Eq. 5.

Table 6 Reference engine SAC parameters calculated at the operating point specified in Sect. 3 (10 km, M = 0.78, 25 kN thrust)

Fuel type	EI_{H2O} (–)	FHV (MJ/kg)	η_o (–)	G (Pa/K)	ALT_C (m)
Kerosene	1.24	43.12	0.37	1.93	9 627
Hydrogen	9.21	118.43	0.37	5.32	8000

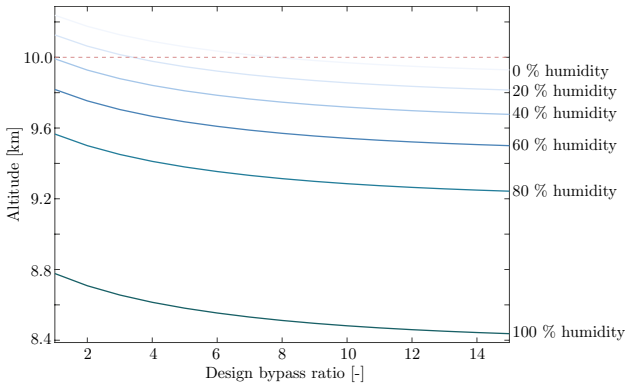

Fig. 6 Critical altitude as a function of the design bypass ratio and ambient humidity for the GTF engine cycle with kerosene. The red dotted line is the cruise altitude. For any part of a curve below this altitude contrails are formed according to the SAC. 0% humidity is irrelevant to the climate impact of contrails and is only included in this study for the sake of completeness. Persistent contrails can form at the altitude of 10 km for ambient humidity with respect to water of more than 60%

4.1 Reference configuration

The mixing lines for kerosene and hydrogen fuel are shown in Fig. 5.

The water emission index of hydrogen is $EI_{H20,H2}$ = 9.21 kg of water/kg of fuel, that of kerosene is $EI_{H20,K}$ = 1.24 kg of water/kg of fuel. The cruise efficiency of the reference engine is η_o = 0.37. Using these values, the mixing line slope G and the critical altitude can be calculated. They are given in Table 6. Hydrogen fuel has a much higher energy-specific water emission index than kerosene, which leads to contrail formation as low as 8000 m for the reference configuration. Both configurations will produce contrails at cruise conditions and 60% ambient humidity with respect to water.

4.2 Geared-turbofan engine cycle

For the GTF engine cycles, we first examined the design bypass ratio with varying humidity. The result for kerosene is shown in Fig. 6. The critical temperature and the critical altitude are influenced by the ambient humidity with respect to water and the slope of the mixing line. With increasing ambient humidity with respect to water, contrails are formed at higher ambient temperatures, resulting in a lower critical altitude.

As stated before, persistent contrails from above 60% ambient humidity with respect to water (> 100% relative humidity with respect to ice). At 60% ambient humidity with respect to water, the critical altitude of a cycle with BPR = 1 is ALT_C = 9.82 km. For BPR = 15, the critical altitude drops to 9.50 km. Greater ambient humidity further decreases the critical altitude. Increasing the bypass ratio increases the engine efficiency, which decreases the critical altitude.

Using hydrogen as a fuel further exacerbates this due to the increased water emission index, as shown in Fig. 7. The critical altitude decreases by around 1.6 km compared to the kerosene configuration. For the BPR = 15 cycle at 60% ambient humidity with respect to water, the critical altitude is 7.89 km.

Figure 8 shows the result of the variation of all the design parameters for a GTF with kerosene as the fuel. Specific thrust is chosen as the x-axis parameter, as this 'expands' the carpet plot and makes the individual data points visible instead of them forming a straight line.

Contrails cannot be avoided for any of the engine cycles examined. The bypass ratio has a greater influence on engine efficiency than the overall pressure ratio and the burner exit temperature. Most modern high-bypass turbofan engines would produce contrails at the cruise conditions examined in this paper. The lowest critical altitude for the GTF engine cycles with kerosene is 9.45 km for BPR = 15, OPR = 70, and T_4 = 1950 K for an engine efficiency of η_o = 0.395. The highest critical altitude achieved is 9.86 km for BPR = 1, OPR = 30, and T_4 = 1950 K for η_o = 0.21. At high bypass ratios and low T_4, the available cycle power is insufficient to accelerate the bypass flow to the optimum exhaust velocity ratio $(V_{18}/V_8)_{id}$. Consequently, no valid solution exists for some parameter combinations, resulting in missing data points in the BPR = 15 carpet.

Figure 9 shows the result of the variation of all the design parameters for a GTF with hydrogen as the fuel.

Similar to the results shown for the kerosene GTF cycle in Fig. 8, contrails cannot be avoided for any of the examined cycles using hydrogen as a fuel. The lowest critical altitude for η_o = 0.41 is ALT_C = 7.83 km for BPR = 15, OPR = 70, and T_4 = 1950 K. The highest critical altitude is 8.33 km for η_o = 0.20 with the cycle design parameters BPR = 1, OPR = 30, and T_4 = 1950 K. The critical altitude for the hydrogen cycle is 1.5 km to 1.6 km lower than for the kerosene cycle, as calculated with the Schmidt–Appleman criterion.

4.3 Open-rotor engine cycle

The open-rotor engine cycle parameters are varied according to Table 4. The critical altitude for the kerosene configuration is shown in Fig. 10. Instead of the specific thrust, the

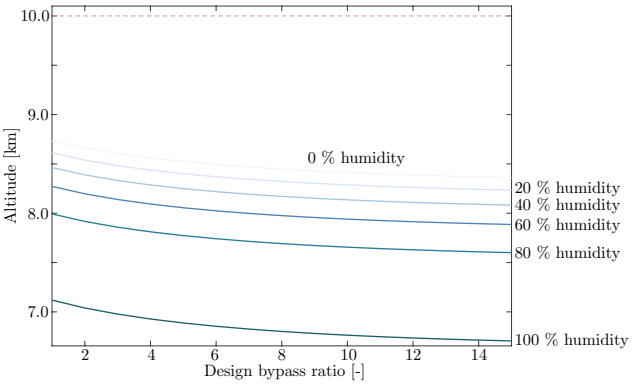

Fig. 7 Critical altitude as a function of the design bypass ratio and ambient humidity for the GTF engine cycle with hydrogen. The red dotted line is the cruise altitude. Similarly to Fig. 6, according to the SAC, the GTF cycles with hydrogen as a fuel will produce contrails at cruise altitude for every examined ambient humidity with respect to water. Persistent contrails form for ambient humidity with respect to water of more than 60%. The lower humidity values are included for the sake of completeness

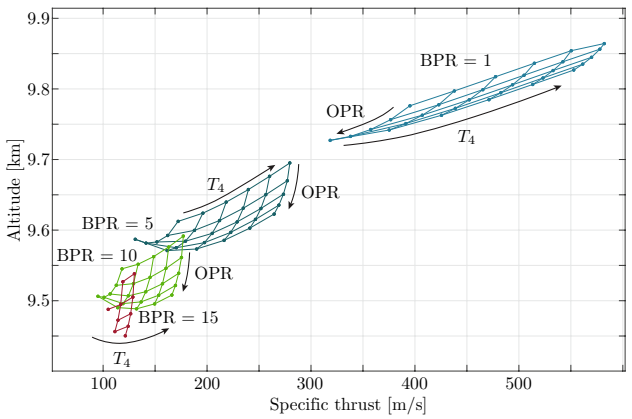

Fig. 8 Critical altitude as a function of design bypass ratio, burner exit temperature, and overall pressure ratio at 60% ambient humidity versus specific thrust. Specific thrust is chosen to make the surface plots clearly distinguishable. OPR increases along the arrow from 30 to 70, T_4 from 1450 K to 1950 K for BPR = 1 and 5. For BPR = 10, valid cycles were only found for $T_4 \geq$ 1550 K. This increases to $T_4 \geq$ 1650 K for BPR = 15. This is due to the chosen optimal V_{18}/V_8 = 0.82. The design bypass ratio is the dominant engine design parameter with respect to critical altitude in this study

specific power is plotted on the x-axis, to expand the carpet plot similarly to the results of the GTF in Sect. 4.2. The highest critical altitude is 9.41 km for OPR = 30, T_4 = 1450 K, and η_o = 0.42. Increasing the OPR decreases the critical altitude. Increasing T_4 also decreases the critical altitude for higher OPR values. The lowest critical altitude for the kerosene open-rotor is ALT_C = 9.25 km for OPR = 70, T_4 = 1950 K at η_o = 0.48. According to the SAC, all kerosene open-rotor engine configurations will produce contrails at the cruising altitude of 10 km.

Similarly to the GTF results, the critical altitude of the hydrogen open-rotor engine configuration is around 1.5 km

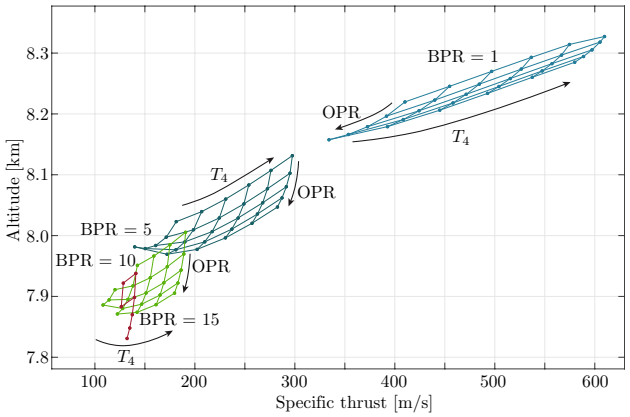

Fig. 9 Critical altitude as a function of design bypass ratio, burner exit temperature, and overall pressure ratio at 60% ambient humidity versus specific thrust for the hydrogen GTF engine cycle. Specific thrust is chosen to make the surface plots clearly distinguishable. OPR increases along the arrow from 30 to 70, T_4 from 1450 K to 1950 K for BPR = 1 and 5. For BPR = 10, valid cycles were only found for $T_4 \geq 1550$ K. This increases to $T_4 \geq 1650$ K for BPR = 15. This is due to the chosen optimal $V_{18}/V_8 = 0.82$. The design bypass ratio is the dominant design parameter with respect to critical altitude in this study

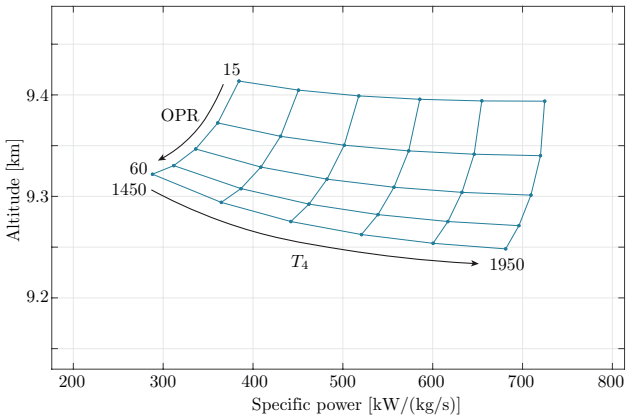

Fig. 10 Critical altitude as a function of the burner exit temperature and overall pressure ratio at 60% ambient humidity versus specific power for the kerosene open-rotor engine cycle. Specific power is chosen to make the surface plots clearly distinguishable. The highest critical altitude is 9.41 km for OPR = 30, T_4 = 1450 K, and η_o = 0.42. The open-rotor engine configuration is more efficient than the GTF configuration due to the increased propulsive efficiency

to 1.6 km lower than that of the kerosene open-rotor engine configuration. The results of the hydrogen open-rotor are shown in Fig. 11.

The highest critical altitude for the hydrogen open-rotor is 7.74 km for OPR = 30 and T_4 = 1450 K at η_o = 0.44. The trends for OPR and T_4 are the same as for the kerosene open-rotor configuration. The lowest critical altitude is 7.54 km for OPR = 70 and T_4 = 1950 K at η_o = 0.5. Again, all hydrogen open-rotor engine configurations will produce contrails at 60% ambient humidity with respect to water at the cruise altitude of 10 km. To avoid contrails, the cruise

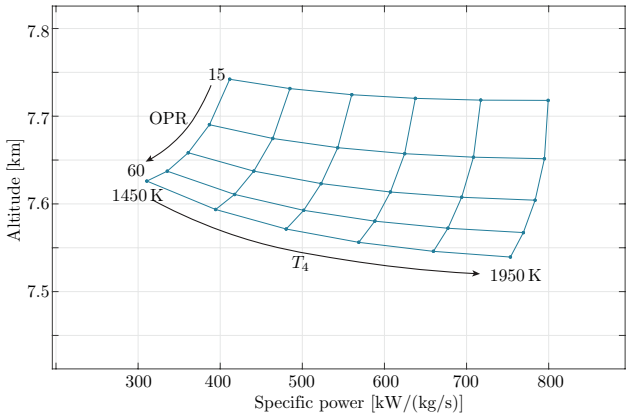

Fig. 11 Critical altitude as a function of the burner exit temperature and overall pressure ratio at 60% ambient humidity versus specific power for the hydrogen open-rotor engine cycle. Specific power is chosen to make the surface plots clearly distinguishable. The highest critical altitude is 7.74 km for OPR = 30, T_4 = 1450 K, and η_o = 0.44

altitude would have to be lowered below the critical altitude for the given engine configuration. It should be noted here that the ambient temperature rises with decreasing altitude. This can raise the temperature above the threshold temperature needed for the contrail to freeze and form cirrus clouds. Therefore, the hydrogen open-rotor may not produce contrails at altitude above the critical altitude as calculated by the SAC. The open-rotor engine configurations all have a lower critical altitude than the GTF configurations. This is due to the increased propulsive efficiency, and thus overall efficiency, of the open-rotor configuration.

4.4 Overall results

The results can be summarised in a single critical altitude plot, as shown in Fig. 12. The x-axis is divided into three groups: the reference configuration, the GTF cycle-adaptation study, and the open-rotor cycle-adaptation study. For the reference configuration, the critical altitude is shown according to Table 6. For the GTF and open-rotor studies, the bars indicate the range of critical altitudes obtained across the investigated design spaces. Hydrogen-fuelled cases are shown in blue and kerosene-fuelled cases in grey/black.

The reference cruise altitude of 10 km is indicated by the red dotted line. Since all calculated critical altitudes lie below this altitude, the Schmidt–Appleman criterion is fulfilled at the reference cruise condition for all investigated configurations.

Accordingly, contrail formation is predicted for all cases at 10 km.

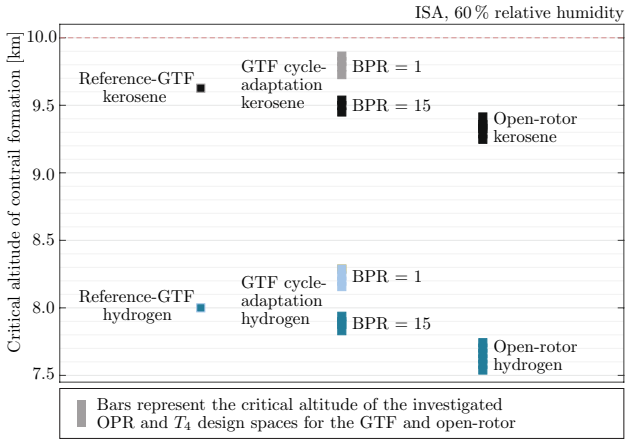

Fig. 12 This figure is a summary of the entire design space shown in Tables 3 and 4 at 60% ambient humidity with respect to water. The critical altitude in the ISA for each engine configuration is represented by the square (single configuration) and rectangular (design space configurations) markers. The critical altitude of the hydrogen cycles (blue hues) is roughly 1.5–1.6 km lower when compared to the kerosene cycles (black and grey hues). More efficient cycles produce contrails at lower altitude. All of the examined engine cycles produce contrails at the cruising altitude of 10 km

5 Discussion and conclusion

Engine cycle adaptations can shift the critical altitude for contrail formation. However, all the critical altitudes of contrail formation of the examined engine cycles are below the cruising altitude of 10 km, when calculating the critical altitude with the Schmidt–Appleman criterion. Thus, all reference, GTF, and open-rotor configurations examined in this study satisfy the Schmidt–Appleman criterion at the reference cruise condition, i.e., they produce contrails at this altitude. Therefore, preventing or avoiding persistent contrails at the cruise altitude of 10 km is not possible with the engine configurations examined. All data on this are provided in the Methodology and Results section.

For the engine configurations considered here, operational altitude changes therefore appear more effective for avoiding persistent contrails than the investigated cycle adaptations alone. For kerosene, the cruise altitude has to be decreased by around 400 m to avoid persistent contrail formation for the reference configuration. For hydrogen, the altitude would have to be decreased by around 2 km according to the SAC, although the SAC has not yet been validated for hydrogen-combusting engines. For more efficient future engine configurations, the altitude correction would have to be 2.5 km for the most efficient hydrogen open-rotor cycles.

It should be noted that the real atmosphere can and does deviate from the ISA conditions. Consequently, aircraft cruising below the ISA-based critical altitude may still produce contrails under actual atmospheric conditions. For operational contrail avoidance, the critical altitude should ideally be evaluated in flight using current atmospheric temperature and relative-humidity data. The results in this paper provide a qualitative measure of how likely the examined engine configurations are to produce contrails.

The calculations used in this paper can be used for future work to develop a robust, low-fidelity framework based on the Schmidt–Appleman criterion to predict whether contrails can form in flight. This information can then be used to calculate the level change needed to prevent persistent contrails from forming. In this context, it is also worth noting that the SAC and the critical altitude describe contrail formation only. Contrail persistence depends on ambient ice-supersaturation conditions, while the actual climate impact further depends on properties such as optical depth and lifetime.

Author contributions J.C. and D.W. wrote the main manuscript text. J.C. prepared figures 1-11 and A1-A4. P.J. provided input for the introduction and methodology sections. All authors reviewed the manuscript.

Funding Open Access funding enabled and organized by Projekt DEAL.

Data availability All data supporting the findings of this study are available within the paper and its Supplementary Information. The engine cycle data are available in tables 1-4 and figures 4-11.

Declarations

Conflict of interest The authors declare no conflict of interest.

Open Access This article is licensed under a Creative Commons Attribution 4.0 International License, which permits use, sharing, adaptation, distribution and reproduction in any medium or format, as long as you give appropriate credit to the original author(s) and the source, provide a link to the Creative Commons licence, and indicate if changes were made. The images or other third party material in this article are included in the article's Creative Commons licence, unless indicated otherwise in a credit line to the material. If material is not included in the article's Creative Commons licence and your intended use is not permitted by statutory regulation or exceeds the permitted use, you will need to obtain permission directly from the copyright holder. To view a copy of this licence, visit http://creativecommons.org/licenses/by/4.0/.

References

1. Lee, D.S., Fahey, D.W., Skowron, A., Allen, M.R., Burkhardt, U., Chen, Q., Doherty, S.J., Freeman, S., Forster, P.M., Fuglestvedt, J., Gettelman, A., León, R.R., Lim, L.L., Lund, M.T., Millar, R.J., Owen, B., Penner, J.E., Pitari, G., Prather, M.J., Sausen, R., Wilcox, L.J.: The contribution of global aviation to anthropogenic climate forcing for 2000 to 2018. Atmos. Environ. **244**, 117834 (2021). https://doi.org/10.1016/j.atmosenv.2020.117834
2. Burkhardt, U., Kärcher, B.: Global radiative forcing from contrail cirrus. Nat. Clim. Chang. **1**, 54–58 (2011). https://doi.org/10.1038/nclimate1068

3. Kärcher, B.: Formation and radiative forcing of contrail cirrus. Nat. Commun. **9**(1), 1824 (2018). https://doi.org/10.1038/s41467-018-04068-0
4. Schmidt, E.: Die Entstehung von Eisnebel aus den Auspuffgasen von Flugmotoren. Schriften der Deutschen Akademie der Luftfahrtforschung **44**(5) (1941)
5. Appleman, H.: The formation of exhaust condensation trails by jet aircraft. Bull. Am. Meteor. Soc. **34**(1), 14–20 (1953)
6. Schumann, U.: On conditions for contrail formation from aircraft exhausts. Meteorol. Z. **5**(1), 4–23 (1996)
7. Schumann, U.: Influence of propulsion efficiency on contrail formation. Aerosp. Sci. Technol. **4**, 391–401 (2000)
8. Schumann, U.: Formation, properties and climatic effects of contrails. C R Phys. **6**, 549–565 (2005)
9. Meerkötter, R., Schumann, U., Doelling, D.R., Minnis, P., Nakajima, T., Tsushima, Y.: Radiative forcing by contrails. Ann. Geophys. **17**(8), 1080–1094 (1999). https://doi.org/10.1007/s00585-999-1080-7
10. van de Hulst, H.C.: Light Scattering by Small Particles. Dover Publications Inc, New York (1957)
11. Minnis, P., Palikonda, R., Walter, B.J., Ayers, J.K., Mannstein, H.: Contrail properties over the eastern north pacific from avhrr data. Meteorol. Z. **14**, 515–523 (2005). https://doi.org/10.1127/0941-2948/2005/0045
12. Ramsay, J., Tristanto, I., Shahpar, S., John, A.: Assessing the impact of turbofan engine design on aircraft contrail properties. ASME J. Eng. Gas Turbines Power **148** (2026)
13. Narciso, M., Sousa, J.M.M.: Influence of sustainable aviation fuels on the formation of contrails and their properties. Energies **14**(17), 5557 (2021). https://doi.org/10.3390/en14175557
14. Yu, F., Kärcher, B., Anderson, B.E.: Revisiting contrail ice formation: impact of primary soot particle sizes and contribution of volatile particles. Environ. Sci. Technol. **58**(40), 17650–17660 (2024). https://doi.org/10.1021/acs.est.4c04340
15. Ponsonby, J., Teoh, R., Kärcher, B., Stettler, M.E.J.: An updated microphysical model for particle activation in contrails: the role of volatile plume particles. Atmos. Chem. Phys. **25**(24), 18617–18637 (2025). https://doi.org/10.5194/acp-25-18617-2025
16. Voigt, C., Märkl, R., Sauer, D., Dischl, R., Renard, C., Seeliger, K., Yu, F., Kaufmann, S., Bräuer, T., Jurkat-Witschas, T., Le Chenadec, G., Moreau, J., Requena-Esteban, E., Bonne, N., Vals, M., Roche, A., Zelina, J., Dörnbrack, A., Eirenschmalz, L., Heckl, C., Horst, E., Lichtenstern, M., Marsing, A., Neumann, G., Roiger, A., Scheibe, M., Stock, P., Giez, A., Eckel, G., Le Clercq, P.: Substantial aircraft contrail formation at low soot emission levels. Nature **652**(8108), 112–118 (2026). https://doi.org/10.1038/s41586-026-10286-0
17. Gierens, K., Lim, L., Eleftheratos, K.: A review of various strategies for contrail avoidance. Open Atmosp. Sci. J. **2**, 1–7 (2008)
18. Teoh, R., Schumann, U., Majumdar, A., Stettler, M.E.J.: Mitigating the climate forcing of aircraft contrails by small-scale diversions and technology adoption. Environ. Sci. Technol. **54**(5), 2941–2950 (2020). https://doi.org/10.1021/acs.est.9b05608
19. Callard, J., Klumpp, C., Weintraub, D., Henninger, S., Jeschke, P.: Reducing contrail formation by engine design and operating point adaptation of aircraft engines. CEAS Aeronaut. J. (2025). https://doi.org/10.1007/s13272-025-00887-2
20. Haglind, F.: Potential of lowering the contrail formation of aircraft exhausts by engine re-design. Aerosp. Sci. Technol. **12**(6), 490–497 (2008). https://doi.org/10.1016/j.ast.2007.12.001
21. Noppel, F., Singh, R., Taylor, M.: Novel engine concept to suppress contrail and cirrus cloud formation. In: Proceedings of the TAC-Conference, pp. 221–240 (2006)
22. Pouzolz, R., Schmitz, O., Klingels, H.: Evaluation of the climate impact reduction potential of the water-enhanced turbofan (wet) concept. Aerospace **8**(3), 59 (2021). https://doi.org/10.3390/aerospace8030059
23. Gao, X., Isoldi, A., Nalianda, D., Nikolaidis, T.: Water extraction in aero gas turbines for contrail mitigation. Aeronaut. J. **128**(1325), 1344–1361 (2024). https://doi.org/10.1017/aer.2024.22
24. Burkhardt, U., Bock, L., Bier, A.: Mitigating the contrail cirrus climate impact by reducing aircraft soot number emissions. NPJ Clim. Atmosph. Sci. (2018). https://doi.org/10.1038/s41612-018-0046-4
25. ...Voigt, C., Kleine, J., Sauer, D., Moore, R.H., Bräuer, T., Le Clercq, P., Kaufmann, S., Scheibe, M., Jurkat-Witschas, T., Aigner, M., Bauder, U., Boose, Y., Borrmann, S., Crosbie, E., Diskin, G.S., DiGangi, J., Hahn, V., Heckl, C., Huber, F., Nowak, J.B., Rapp, M., Rauch, B., Robinson, C., Schripp, T., Shook, M., Winstead, E., Ziemba, L., Schlager, H., Anderson, B.E.: Cleaner burning aviation fuels can reduce contrail cloudiness. Commun. Earth Environ. (2021). https://doi.org/10.1038/s43247-021-00174-y
26. Williams, V.: The engineering options for mitigating the climate impacts of aviation. Philos. Trans. Ser. A Math. Phys. Eng. Sci. **365**(1861), 3047–3059 (2007). https://doi.org/10.1098/rsta.2007.0012
27. ICAO: Manual of the ICAO Standard Atmosphere: extended to 80 km. (DOC7488/3 262 500 feet) (1993)
28. Wilkerson, J.T., Jacobson, M.Z., Malwitz, A., Balasubramanian, S., Wayson, R., Fleming, G., Naiman, A.D., Lele, S.K.: Analysis of emission data from global commercial aviation: 2004 and 2006. Atmos. Chem. Phys. **10**, 6391–6408 (2010)
29. International Civil Aviation Organization (ICAO) Engine Emissions Databank, Cologne (2025)
30. Daly, M.: Jane's Aero-Engines. Coulsdon Surrey, London (2014)
31. GasTurb GmbH: GasTurb 15. GasTurb GmbH (2025)
32. Saravanamuttoo, H.I.H., Rogers, G.F.C., Cohen, H.: Gas Turbine Theory, 12th edn. Dorling Kindersley, New Delhi (2013)
33. Mattingly, J.D.: Elements of Gas Turbine Propulsion. Tata McGraw, New Delhi (2005)
34. Sonntag, D.: Fortschritte in der Hygrometrie. Meteorol. Z. **3**(2), 51–66 (1994). https://doi.org/10.1127/metz/3/1994/51

Publisher's Note Springer Nature remains neutral with regard to jurisdictional claims in published maps and institutional affiliations.